

Article

# Topology Comparison Study of Five-Phase Wound-Field Doubly Salient Fault Tolerant Generators

Liwei Shi \*, Junhao An and Wenchao Zhang

School of Transportation and Vehicle Engineering, Shandong University of Technology, Zibo 255000, China; anjunhao829@163.com (J.A.); Icezz1X@163.com (W.Z.)

\* Correspondence: liwei10@nuaa.edu.cn; Tel.: +86-278-6837

Received: 21 April 2019; Accepted: 20 May 2019; Published: 23 May 2019



**Abstract:** To present the characteristics of pole number and pole shape of the core, the five-phase wound-field doubly salient generators (WFDSGs) with symmetric phase inductance are studied and optimised in this paper, considering the split ratio, slot fill factor and core fringing effect. Based on the principle and structure of the five-phase WFDSGs, the winding induced electro-motive force under different number of poles is theoretically analysed. The constraints for parameter optimisation design including slot fill factor, split ratio and magnetic density characteristic are given. The finite element models of 30/24-pole and 20/16-pole WFDSG are established, and the comparative simulation analysis is carried out. It is pointed out that when the inner and outer diameters of the stator and rotor, the axial length and the maximum magnetic density are constant, the induction electromotive forces of the WFDSGs with different pole numbers and same phase coil number are same. Considering the pole fringing effect, the rotor pole equivalent width is the sum of the rotor pole actual width and 4 times of the air gap. The comparison experiments between the 30/24-pole and 20/16-pole WFDSGs were carried out, which verified the correctness of the theoretical analysis and finite element analysis (FEA).

**Keywords:** doubly salient electromagnetic machine; generator; fault-tolerant; multi-phase

## 1. Introduction

With the continuous development of science and technology, more and more devices are beginning to shift from full-size to micro-sized portable, and small-scale energy conversion devices are being gradually developed and applied [1,2]. The integrated internal combustion engine and generator as a universal power constitute an independent power generation system. In order to meet the rapid development of portable electronic products and MEMS, it is of great theoretical and practical significance to develop a small internal combustion engine power generation system [3]. As the core component of the electric power system, the reliability of the generator directly affects the performance of the power system. Aircrafts, automobiles, and other transportation vehicles have higher and higher reliability requirements for the electric power systems [4–7]. In these applications where reliability is critical, the generator is required to have fault tolerance for normal or low grade performance in the event of a fault [8–10].

The multiphase electric machines with more than three phases are very suitable to be used in high reliability situations because they can limp operate even with one or two open-circuited phases [11,12]. Recently, most of the studies have concentrated on the multiphase driving motors and their fault-tolerant inverters and controllers [13,14], which have shown the multiphase machine improve the fault tolerance performance of the traditional motors.

For the generators at present, the aircrafts usually use three-stage synchronous machines, permanent magnet synchronous machines, and switched reluctance machines, etc. The rotor of

the three-stage synchronous machines has the three-phase windings and rotating rectifiers of an AC exciter. And the stator also has three-phase windings of the permanent magnet auxiliary exciter and excitation windings of the AC exciter. The overall structure of the machine is complicated and the cost is high [15]. Permanent magnet synchronous generator also has shortcomings, such as difficulty in voltage regulation and flux-weakening in failure condition, especially at high-speed [16,17]. When the switched reluctance machine is used as a generator, the voltage control is more complicated than the wound field machine in controlling the phase current, and a larger filter circuit is needed [18,19]. Most of the generators used in automobiles are claw pole alternators [20]. The machine is generally structured with a carbon brush and slip ring, and the carbon brush on slip ring is easy to wear out, which is not conducive to the reliability of the automobile generator.

Compared with the above generators, the wound-field doubly salient generator (WFDSG) has a simple and reliable rotor with salient-poles, as well as a field winding capable of regulating voltage [21]. Moreover, the position sensors are not needed for power generation operation, and the excitation current can be directly adjusted like the wound-field synchronous generator to keep the output voltage stable, and the voltage regulation performance is good, which is very suitable as a generator [22–25]. For example, a three-phase WFDSG is used to construct a brushless DC extended-range power generation system for electric vehicles in [26], and the power generation control strategy is proposed.

In addition to the abovementioned low failure rate, high-reliability generators should also have the ability to operate under fault conditions. Conventional generators with three-phase star windings do not operate properly with a single-phase fault. Electric generators structured with multi-phase or redundant channel can achieve certain output after single-phase or single-channel faults by using multi-phase or redundant channel windings, which have fault tolerance or additional capacity [27–29]. For the multi-phase generator, it reduces the voltage ripple rate after rectification because of the electric angle of the electromotive force (EMF) waveforms are larger than  $120^\circ$ .

To play the advantages of doubly salient brushless generator and multi-phase generator, [30] proposed the fault-tolerant performance of a traditional five-phase WFDSG and verified that the generator has good fault-tolerant performance. This traditional five-phase WFDSG has five armature windings for each excitation coil, and there is a certain difference in the flux linkage and inductance amplitude of each phase [31]. To realize the symmetry of the flux linkage of each phase of the five-phase WFDSG, a new winding configuration wound on 30/24-pole was proposed in [32]. And it was proved that the machine has good fault tolerant performance.

However, there is still lack of theoretical analysis of the influence of the main core parameters considering the pole number, slot fill factor, and split ratio with the same stator outer diameter, especially the pole structure optimization analysis considering the fringing effect of the five-phase WFDSG. The core parameters including pole numbers and pole shape of the five-phase WFDSG have significant impact on their characteristics [33]. In order to conclude the influence of the main core parameters mentioned above, this paper describes the principle and topology of a five-phase WFDSG. The winding induced electro-motive force under different number of poles and the impact of major core parameters are theoretically analysed. And then compares the 30/24-pole and 20/16-pole WFDSGs with FEA method. The equivalent width of the rotor pole considering the fringing effect is analysed with theoretical analysis and finite element method. Finally, two prototypes were prototyped and experimentally verified to verify the correctness of theoretical analysis and finite element analysis. The finding in this study can be used as a design theory for a five-phase WFDSG that may optimize generator performance.

## 2. Topology and Principle of the Five-Phase WFDSG

In the conventional five-phase WFDSGs, each excitation coil is wound across five stator poles. The stator pole number should be an even multiple of the phase number 5, that is, the minimum unit machine is a 10/8 pole structure. Literature [32] has pointed out that the traditional five-phase WFDSG

has an amplitude difference in the inductance of each phase, and this asymmetry in the inductance of each phase will result in asymmetrical phases, which will increase the unbalanced phase load.

Formula for ratio of stator pole number to rotor pole number of five-phase WFDSG [32]:

$$\frac{p_s}{p_r} = \frac{5}{4} \text{ or } \frac{5}{6}. \tag{1}$$

The symmetry of each phase winding can be achieved by changing the number of poles wound by the field winding. When each field winding is wound across 2 stator poles, the number of stator poles is at least 20. If each field winding is wound across 3 stator poles, the stator pole number is at least 30. For the WFDSG with inner rotor, the number of rotor poles is usually less than the number of stator poles. Therefore, two kinds of five-phase WFDSGs can be proposed, one has 30 stator pole and 24 rotor poles, which is summarized as 30/24-pole, and the other is structured with 20/16-pole, as shown in Figure 1.

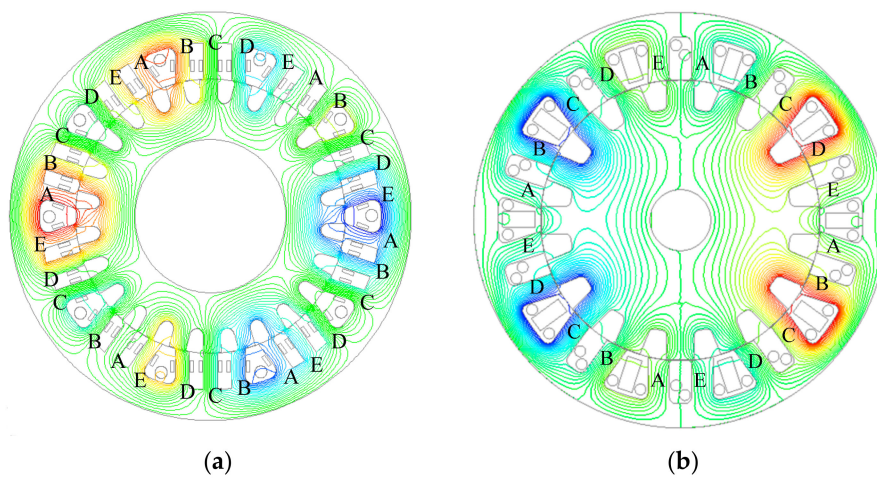


**Figure 1.** Two topology of the five-phase wound-field doubly salient generators (WFDSGs). (a) 30/24-pole; (b) 20/16-pole.

When the excitation current of the five-phase WFDSG is turned on, the excitation magnetic field is established inside the machine. When the five-phase WFDSG armature winding and the excitation winding are all conducted with currents, the flux linkage of the armature winding and the excitation winding can be expressed by the following formula:

$$[\psi] = [L][I], \tag{2}$$

where the matrix  $[\psi]$ ,  $[L]$ , and  $[I]$  represent the flux linkage, inductance, and current matrix, respectively, and the subscripts a, b, c, d, e, and f correspond to phase A, phase B, phase C, phase D, phase E, and field winding.

$$[\psi] = [\psi_a, \psi_b, \psi_c, \psi_d, \psi_e, \psi_f]' \tag{3}$$

$$[L] = \begin{bmatrix} L_a & L_{ab} & L_{ac} & L_{ad} & L_{ae} & L_{af} \\ L_{ba} & L_b & L_{bc} & L_{bd} & L_{be} & L_{bf} \\ L_{ca} & L_{cb} & L_c & L_{cd} & L_{ce} & L_{cf} \\ L_{da} & L_{db} & L_{dc} & L_d & L_{de} & L_{df} \\ L_{ea} & L_{eb} & L_{ec} & L_{ed} & L_e & L_{ef} \\ L_{fa} & L_{fb} & L_{fc} & L_{fd} & L_{fe} & L_f \end{bmatrix} \tag{4}$$

$$[I] = [i_a, i_b, i_c, i_d, i_e, i_f]' \tag{5}$$

Because the armature windings of the WFDSG are concentrated windings wound in the same direction, and the numbers of phase turns are much smaller than the excitation winding, the mutual inductance flux linkage is small, and the mutual inductance between the armature windings can be neglected, and the flux linkage equation can be rewritten as:

$$\begin{bmatrix} \psi_a \\ \psi_b \\ \psi_c \\ \psi_d \\ \psi_e \\ \psi_f \end{bmatrix} = \begin{bmatrix} L_a & 0 & 0 & 0 & 0 & L_{af} \\ 0 & L_b & 0 & 0 & 0 & L_{bf} \\ 0 & 0 & L_c & 0 & 0 & L_{cf} \\ 0 & 0 & 0 & L_d & 0 & L_{df} \\ 0 & 0 & 0 & 0 & L_e & L_{ef} \\ L_{fa} & L_{fb} & L_{fc} & L_{fd} & L_{fe} & L_f \end{bmatrix} \begin{bmatrix} i_a \\ i_b \\ i_c \\ i_d \\ i_e \\ i_f \end{bmatrix} \quad (6)$$

From Equation (4), it can be seen that the mutual inductance between the five-phase windings of the generator is small, the five-phase windings are relatively independent, and have strong isolation characteristics. The failure of one or more phases has little effect on the remaining phases. Therefore, the five phases of the generator can simultaneously output current independently and have strong fault tolerance.

### 3. Comparative Study and Simulation of Five-Phase WFDSG

In order to present the optimized core parameters of the five-phase WFDSG, three parts are described in this section. Section 3.1. shows the slot fill factor, split ratio, and magnetic density characteristic constraints. Section 3.2. is the comparative study of two WFDSGs with 30/24-pole and 20/16-pole. And the rotor pole is optimized considering the fringing effect with equivalent width analysis and FEA method in Section 3.3.

#### 3.1. WFDSG Design Constraints

Although the new five-phase WFDSG differs from the conventional machine in structure and principle, the WFDSG still conforms to the general law of electromechanical energy conversion, and the basic parameters of the WFDSG can still be analysed by the electromagnetic formula of the electric machine. Let the output capacity of the machine be:

$$P = mui. \quad (7)$$

Here,  $m$  is the number of phases,  $u$  and  $i$  are the voltage and current of each phase. Ignoring the effect of the saturation effect, the voltage waveform of the five-phase WFDSG can be regarded as a square wave, and its peak value  $u_{\max}$  can be calculated as:

$$u_{\max} \approx N_p(\phi_{\max} - \phi_{\min}) \frac{np_r}{60} \frac{360}{\theta}. \quad (8)$$

Here,  $N_p$  is the total turn number of the series connected phase turns,  $n$  is the number of stator poles and rotor poles overlapping,  $\phi_{\max}$  is the maximum value of the phase flux linkage,  $\phi_{\min}$  is the minimum value of the phase flux linkage,  $\phi_{\max} = \alpha_s \tau_s LB_s$ .  $\alpha_s$  is the stator pole arc coefficient,  $\tau_s$  is the stator pole pitch,  $\tau_s = \pi D/p_s$ .  $D$  and  $L$  are the air gap diameter and the core length of the WFDSG. The electrical angle corresponding to the rising interval of the inductor is  $\theta$ .

$$\theta = \frac{360^\circ \alpha_s}{p_s} p_r. \quad (9)$$

Let the magnetic flux leakage coefficient  $k_d$ :

$$k_d = \frac{(\phi_{\max} - \phi_{\min})}{\phi_{\max}}. \quad (10)$$

Substituting Equation (8) and  $k_d$  into Equation (7), and then Equation (7) can be calculated as:

$$u_{\max} \approx \frac{\pi k_d D N_p L B_\delta n}{60} \tag{11}$$

It can be seen from Equation (9) that by adjusting the magnitude of the excitation current, the air gap magnetic field can be adjusted to achieve the purpose of keeping the output voltage stable. At the same time, since there is no pole number and pole arc coefficient in Equation (9), changing the pole number and pole arc coefficient has no effect on the peak value of the output voltage, under the condition of neglecting magnetic flux leakage and magnetic saturation. This is because although a large number of poles increase the frequency, it also reduces the magnetic flux per pole.

Transform Equation (9), and the formula of the armature winding turns can be calculated as:

$$N_p \approx \frac{60 u_{\max}}{\pi k_d D L B_\delta n} \tag{12}$$

Therefore, it can be seen that in the case where the external dimensions of the WFDSG and the magnetic gap of the air gap are constant, the output voltage of different WFDSGs are the same if they have the same total turns number of the armature windings in each phase.

The design requirement of the field winding of the five-phase WFDSG is to sufficiently provide enough field magnetizing. In the case of instauration, the magnetic force of the core is relatively small. Therefore, according to the second law of Kirchhoff and the size of the air gap, the excitation magnetic potential can be calculated, and then the required excitation slot area can be calculated according to the winding current density.

The design method of the armature winding and the field winding given above can be used to calculate the slot fill factor of the WFDSG core. The design optimization of the WFDSG parameter should consider the following constraints:

$$\left\{ \begin{array}{ll} \text{Split ratio :} & \gamma = \frac{D}{D_0} < 1 \\ \text{Diameter :} & D_0 - D = 2(h_c + h_e) \\ \text{Second air gap :} & h_c > 6mm \\ \text{Stator yoke :} & h_e \geq \frac{\pi D \alpha_s}{p_s} = b_c \\ \text{Field slot fill fator :} & \frac{N_f d_f^2 + 2N_p d_p^2}{\frac{\epsilon}{360} \pi (D_0 - 2h_e - h_c) h_c} \leq 0.6 \\ \text{Armature slot fill fator :} & \frac{2N_p d_p^2}{\frac{\epsilon}{360} \pi (D_0 - 2h_e - h_c) h_c} \leq 0.5 \end{array} \right. \tag{13}$$

where,  $\gamma$  is the split ratio of the WFDSG,  $D_0$  and  $D$  are the out diameter and air gap diameter,  $h_e$  and  $h_c$  are the teeth height and yoke height of the stator, and  $b_c$  is the teeth width of the stator.  $N_f$  and  $d_f$  are excitation winding turns and diameter per slot,  $N_p$  and  $d_p$  are armature winding turns and diameter per slot,  $\epsilon$  is the mechanical angle at which the center line of the field slot is the center of the arc and the circle is the center of the circle, and  $\epsilon$  is the mechanical angle at which the center line of armature slot is the center of the arc and the circle is the center of the circle. And the second air gap is the distance between rotor yoke and stator pole.

In the case where the outer diameters of the WFDSGs are equal, the larger the air gap diameter  $D$  is, the larger the magnetic flux of the core and the higher power it can provide. However, with the increase of the split ratio, the slot area will shrink when the winding turns and wire diameter are fixed, and the slot fill factor of the WFDSG will increase [29]. The split ratio can be enlarged if the number of poles increases. On the other hand, the stator teeth and the stator yoke will be too thin to cause fatigue fracture if the pole number is too large.

Similarly, if the diameters of the field winding and armature winding decrease, the split ratio of the WFDSG can be enlarged. However, if the diameters of the field winding and the armature winding

are too small, the internal resistance of the winding will be too large to keep the winding in normal temperature. Anyway, the diameters of the field winding and the armature winding are limited by the excitation current and the armature current.

### 3.2. The Comparative Analysis of Two WFDSGs

Considering the influence of the windings on the core, two WFDSG with 30/24-pole and 20/16-pole were comparatively studied, the parameters are shown in Table 1. The field slot fill factor usually used is not more than 0.5, and it is slightly more difficult to wind.

**Table 1.** Parameters of five-phase WFDSG.

Item	30/24-pole	20/16-pole
Stator/rotor pole number	30/24	20/16
Number of turns per phase	6 × 6	9 × 4
Poles wound by an excitation coil	3	2
Number of turns/excitation winding	60 × 10	60 × 10
Stator yoke thickness (mm)	9	7.5
Field slot fill factor (%)	55.4	48.4
Armature slot fill factor (%)	26.7	30.6
Rotor pole arc coefficient	0.5	0.45
Outer diameter of the stator (mm)	136	
Inner diameter of the stator (mm)	92	
Air-gap (mm)	0.3	
Iron stack length (mm)	40	
Core iron	DW470-50	

According to Table 1, the simulation models five-phase 30/24-pole and 20/16-pole WFDSG are established by using the magnetic field finite element software. The simulated no-load magnetic field distribution is shown in Figure 1.

When the speed is 3000 r/min, the simulated no-load electromotive force is shown in Figure 2a,b. It can be seen from the waveforms that the five-phase WFDSG is different from the conventional generator. The electromotive force waveform has a flat top width of about 144° electrical angle, and the phase difference between two adjacent phases is 72°. At any time, there are two phases with positive or negative voltages at the same time, which is a backup supply for each other.

Figure 2c,d show the flux linkages of the two WFDSG with a field current of 3A. It can be seen from the waveform that the magnitudes of the flux linkages of the 30/24-pole and 20/16-pole five-phase doubly salient electromagnetic machine (DSEM) are equal, and they are symmetrical phases.

Since the two WFDSGs have the same number of excitation amps and the total turn numbers of the armature windings are equal, the magnitude of the flux linkage and the magnitude of the EMF are similar at the same speed, which is consistent with Equation (11). However, due to the small distance between two poles, the leakage effect of the 30/24-pole WFDSG is larger than that of the 20/16-pole one, and the minimum flux linkage and the EMF amplitude are slightly smaller, too. When the inner and outer diameters of the stator and rotor, as well as the axial length and the maximum magnetic density, are constant, the EMFs of the WFDSGs with different pole numbers and the same phase coil number are almost equal.

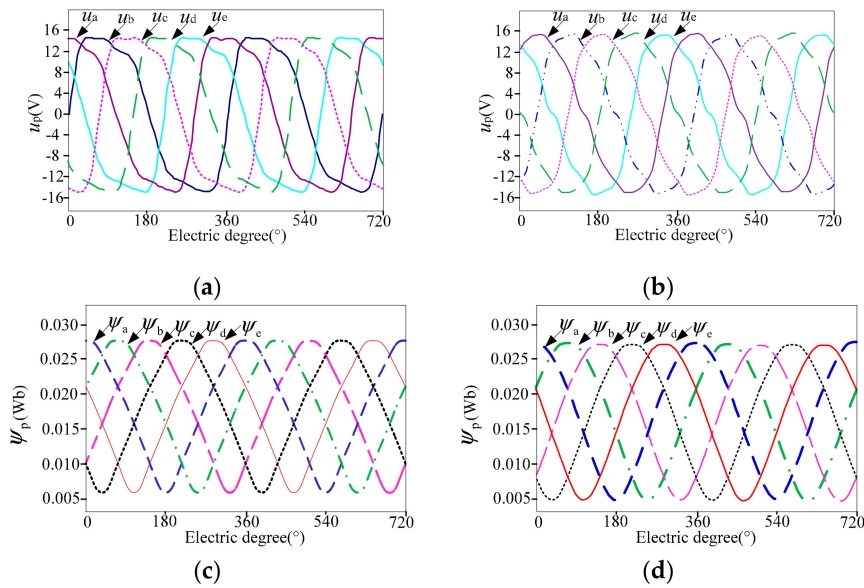


**Figure 2.** The simulated electromotive force (EMF) and flux linkage. (a) Phase EMF of 30/24-pole. (b) Phase EMF of 20/16-pole. (c) Phase flux linkage of 30/24-pole. (d) Phase flux linkage of 20/16-pole.

### 3.3. Rotor Pole Optimization Considering the Fringing Effect

Ignoring the core fringing effects, the peak and valley lengths of the inductance waveforms of each phase should be equal when the stator pole arc coefficient  $\alpha_r = 0.5$ . According to the inductance and back EMF characteristics of the five-phase WFDSG, the back EMFs of the machine are also approximately square waves.

However, due to the core fringing effect, the magnetic flux is conducting before the stator and rotor poles start to slip together, as shown in Figure 3. Since the principle is similar to the actual length of the iron core in the machine design, it can be used to refer to the definition of the equivalent length of the core in the machine design. Here, let the rotor pole arc equivalent length  $l_{rpe}$  be the performance functional pole arc length, and it is larger than the rotor pole arc actual length  $l_{rp}$ , as shown in Figure 3.

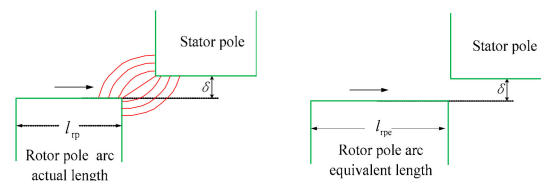


**Figure 3.** Rotor pole equivalent length.

In order to obtain the rotor pole arc actual length that has the best output performance of the WFDSG, let:

$$l_{rp} = l_{rpe} - z\delta, \tag{14}$$

where  $z$  is the unknown number to be solved, and  $\delta$  is the air gap length.

For a five-phase WFDSG, when the peak and valley lengths of the inductance waveforms of each phase are equal,  $\alpha_r = 0.5$ , the ideal value of the equivalent arc length of the rotor should be:

$$l_{rpe} = 0.5 \frac{\pi D}{p_r} = \frac{\pi D}{2p_r}. \tag{15}$$

In order to obtain the optimized  $z$  in Equation (12), the method of intersecting two rotor cores in the simulation software is used to establish a 20/16-pole five-phase WFDSG optimisation model. When  $z$  is selected from 0 to 5, the flux linkage, no-load EMF and cogging torque of phase A were

simulated [34]. And the waveform diagrams and harmonic diagram were obtained as shown in Figure 4.

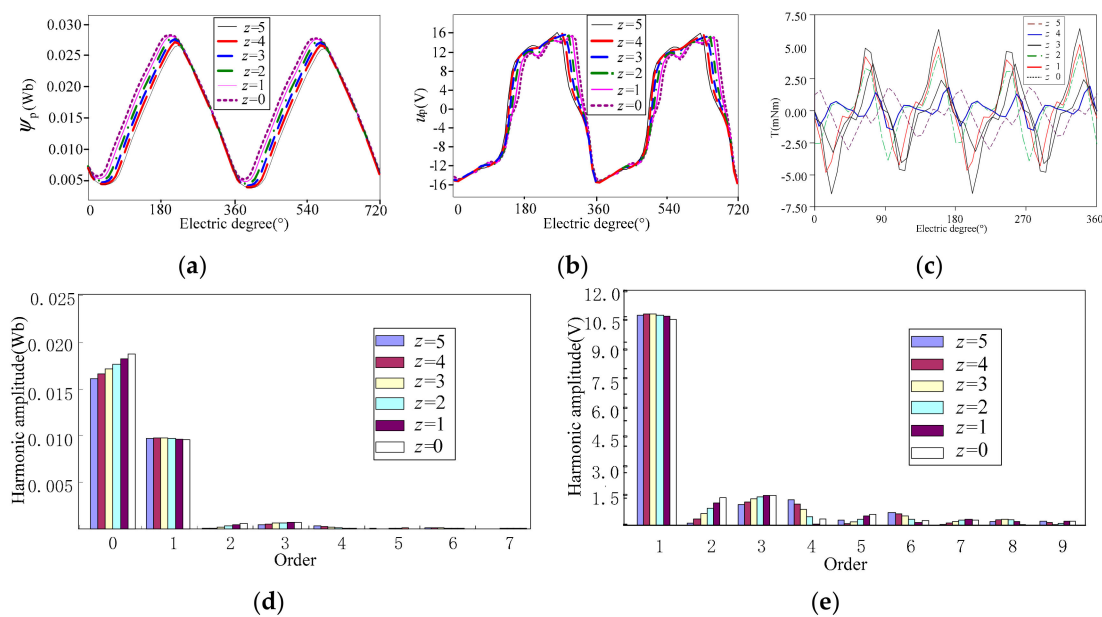


**Figure 4.** Influence of rotor arc length on WFDSGs. (a) Flux linkage when excitation current is 5A; (b) EMF when excitation current is 5A; (c) the cogging torque when excitation current is 1A; (d) harmonics of the flux linkage and (e) harmonics of the EMF.

It can be seen that the arc length of the rotor has a direct influence on the peak and valley length of the flux linkage, as well as affects the induced EMF waveforms. When the arc length of the rotor changes within the above range, the amplitudes of no-load induced EMF are almost equal. As  $z$  gradually decreases from 4 to 0, the rotor pole actual length gradually approaches the ideal pole arc length in Equation (13), the fundamental wave content of the no-load EMF and the flux linkage gradually decrease. On the other hand, if  $z$  is increased to 5, the rotor pole length is smaller than the ideal pole arc length in Equation (13), and fundamental wave content of the no-load EMF and the flux linkage are also smaller than that of  $z = 4$ . In summary, when  $z = 4$ , the fundamental wave content of each phase flux and no-load EMF is the largest.

In the cogging torque waveform showed in Figure 4c, when  $z$  gradually decreases from 4 to 0, the cogging torque increases correspondingly. When  $z = 5$ , the cogging torque is also relatively large. The minimum cogging torque is achieved when  $z = 4$ . This is also consistent with the above fundamental wave content analysis. Therefore, when the rotor pole arc length  $l_{rp}$  is  $4\delta$  narrower than the ideal pole arc length, the cogging torque of the five-phase WFDSG is the smallest, the flux linkage and no-load EMF harmonic content are also the smallest.

Overall, for five-phase WFDSG, considering the pole fringing effect, to get the low cogging torque, as well as the harmonic content of phase flux and EMF, the peak of each phase inductance is equal to the trough length  $\alpha_r = 0.5$ , the rotor pole equivalent width is the sum of the rotor pole actual width and four times that of the air gap.

In the traditional machine design [35], if the axial length of the stator core and the rotor core are the same, and the leakage flux between the rotor pole and the stator pole only passes through the end face. And the equivalent length of the core is usually calculated as the sum of the axial length of the stator core and double air gap. For the WFDSG, the rotor poles and the stator poles are gradually approaching and meshing at both ends. Not only the side of the rotor pole has magnetic lines of force, but also the side of faces of the stator pole have magnetic lines of force, so the magnetic flux leakage between the stator pole and the rotor pole is twice that of their alignment.

In summary, the rotor pole equivalent width is the sum of the rotor pole actual width and the four times air gap. The above results are consistent with the empirical formula for the equivalent axial length of the stator core in the traditional machine design.

#### 4. Experimental verification

In order to verify the above theoretical analysis, two five-phase WFDSGs were prototyped and tested, and the WFDSGs are shown in Figure 5  $\alpha_r = 0.5$ .

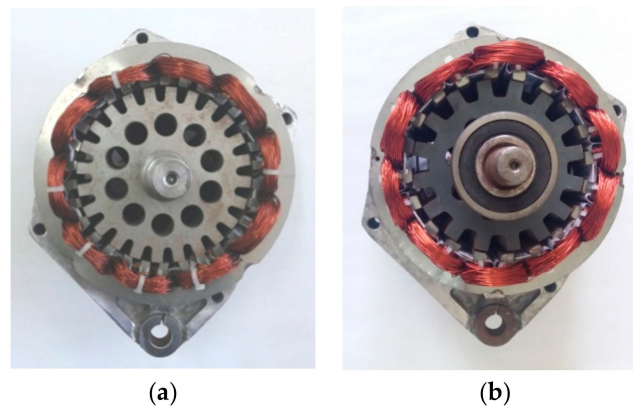


**Figure 5.** The rotor and stator of the five-phase WFDSGs. (a) 30/24-pole; (b) 20/16-pole.

Figure 5a,b shows the excitation coil and armature coil on the stators of the two five-phase WFDSGs, respectively, which realize brushless excitation. And without winding and permanent magnet, the rotor structure is simple and suitable to operate in high temperature and high-speed situations. In addition, the windings of each phase on the stator are physically and electromagnetically independent, which enables the WFDSG with isolation and fault tolerance characteristics. In Figure 6, a five-phase rectifier and a regulator are used to output steady DC voltage by adjusting the excitation current.

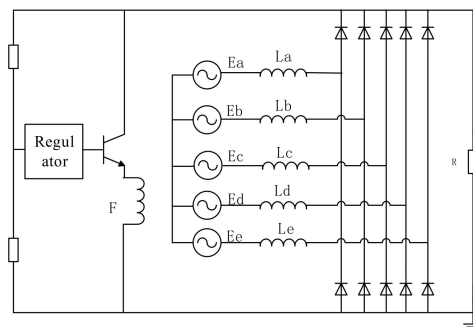


**Figure 6.** The five-phase rectifier and excitation of the WFDSG.

With the same parameters as the simulation, the normal and the single-phase open-circuit experiment of the two prototypes were carried out. The no-load EMFs of the two WFDSGs are shown in Figure 7a,b. The phase EMFs and the output EMFs of the one phase open-circuit are shown in Figure 7c,d, which show output DC voltage ripple of the 20/16-pole WFDSG is less than that of the 30/24-pole WFDSG. The experimental waveforms of the phases are consistent with the simulated waveforms.

With a regulator, in the case of unsaturated excitation, if the 20/16-pole WFDSG has a single-phase open-circuit fault, the regulator automatically increases the excitation current to stabilize the output voltage for charging the battery, as shown in Figure 7e.

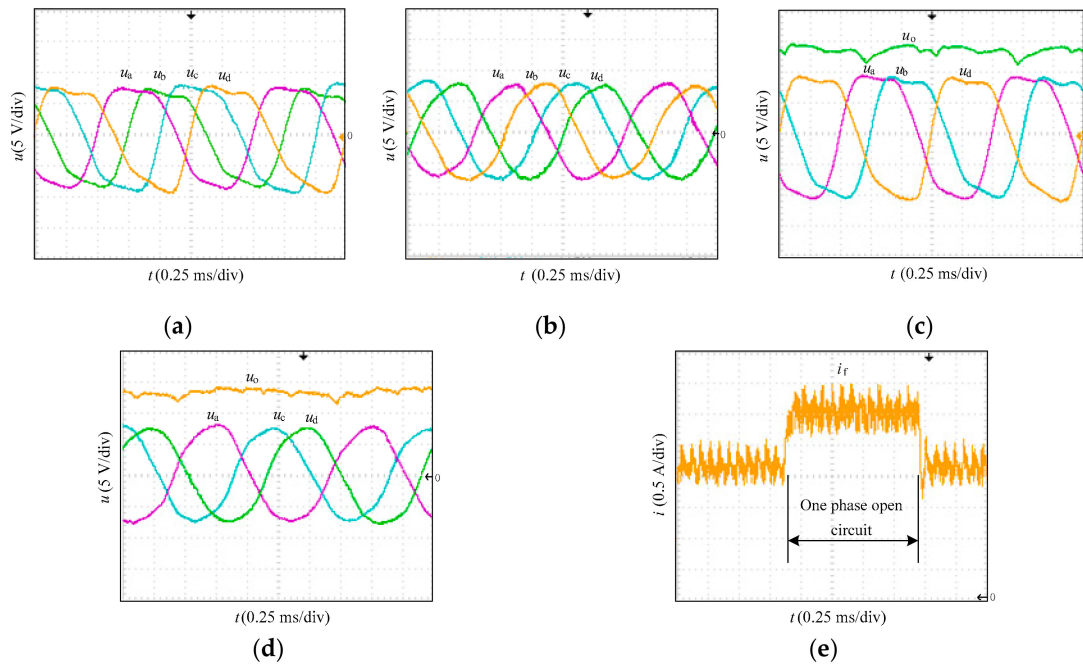


**Figure 7.** The normal and one phase open-circuit experiment waveforms. (a) Normal no-load EMF of the 30/24-pole WFDSG; (b) normal no-load EMF of the 20/16-pole WFDSG; (c) no-load EMF with one phase open-circuit of the 30/24-pole WFDSG; (d) no-load EMF with one phase open-circuit of the 20/16-pole WFDSG; and (e) excitation current with one phase open-circuit.

If the 30/24-pole and 20/16-pole WFDSGs are connected with the loads of 0.5, 1, 2, 4, and 15 ohm, the external characteristics and output characteristics can be drawn as shown in Figure 8.

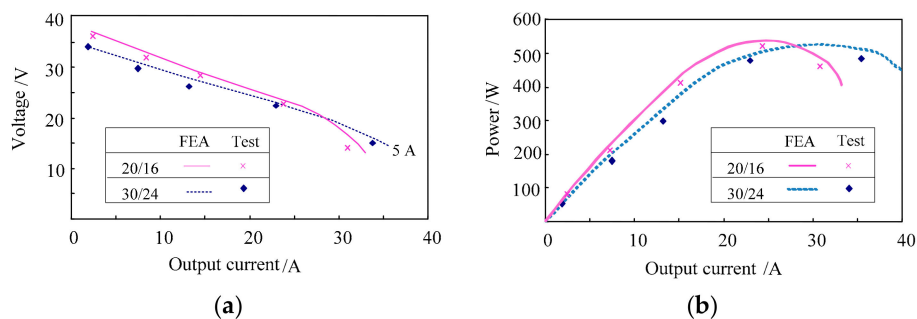


**Figure 8.** External and output characteristics. (a) External characteristics and (b) output characteristics.

Comparing the external and output characteristics of the two WFDSGs, it can be seen that the output voltage and output power of the 20/16-pole WFDSG are larger than the 30/24-pole when the output current is less than 27A, which is also consistent with the simulation results, and this verifies the increase in the number of poles will deduce the second air gap and increase the leakage coefficient of the WFDSG. When the output current is larger than 27A, the output voltage and output power of the 20/16-pole WFDSG drop sharply due to the large demagnetization effect of the armature reaction because there are more turns of the armature winding around each pole of the 20/16-pole WFDSG. Although the armature reaction sometimes enlarges the excitation flux and sometimes reduces it, in the case of almost saturation excitation, the enlargement is difficult to increase the magnetic density of the core, but the demagnetization of the armature reaction can reduce the magnetic density of the core [36].

Overall, the experimental results agree well with the simulation results, but the experimental data is slightly lower than the simulation data due to the influence of materials and production.

## 5. Conclusions

To present the characteristics of pole number and pole shape of the core, the five-phase Wound-field Doubly Salient Fault Tolerant Generators with symmetric phase inductance were studied and optimised in this paper, considering the split ratio, slot fill factor and core fringing effect. Two 30/24-pole and 20/16-pole Wound-field Doubly Salient Fault Tolerant Generators with low harmonic were proposed and analysed with theoretical analysis and finite element analysis method. And with the finite element analysis and experimental results, the conclusion can be drawn as follows:

1. If the other parameters are equal, the output voltages of Wound-field Doubly Salient Fault Tolerant Generators with different poles are equal if they have the same total turn number of the armature windings. However, the pole to pole leakage effect of the 30/24-pole Wound-field Doubly Salient Fault Tolerant Generator is larger than that of the 20/16-pole, which decreases the flux linkage and the EMF amplitude. Since the number of stator poles is larger than the number of rotor poles, the stator slots are narrower than the rotor slots when the stator and rotor pole arc coefficients are the same, so the equivalent air gap length is also small. Similarly, the narrower the stator slot and the rotor slot, the smaller the equivalent air gap length of the stator slot and the rotor slot, that is, the larger the leakage magnetic flux.
2. Considering the core fringing effect, to reduce the cogging torque, as well as the harmonic content of phase flux and electromotive force, the rotor pole arc actual length should be four times the length of the air gap narrower than the ideal pole arc length. Under this circumstance, the five-phase Wound-field Doubly Salient Fault Tolerant Generator studied in this paper has the smallest harmonic content of the flux linkage and no-load electromotive force, and the minimum positioning torque is the ideal design target of the rotor pole arc length.
3. Although the total phase turn numbers are the same, the output power of the 30/24-pole Wound-field Doubly Salient Fault Tolerant Generator is smaller than the 20/16-pole one when the output current is smaller than 27A, due to the demagnetisation effect of the armature reaction. Due to the pole to pole leakage flux, the output power of the 30/24-pole Wound-field Doubly Salient Fault Tolerant Generator is larger than the 20/16-pole one when the output current is larger than 27A. The 20/16 pole Wound-field Doubly Salient Fault Tolerant Generator drops sharply due to the large demagnetization effect of the armature reaction because there are more turns of the armature winding around each pole of the 20/16-pole Wound-field Doubly Salient Fault Tolerant Generator. And this verifies the increase in the number of poles will deduce the second air gap and increase the leakage coefficient of the Wound-field Doubly Salient Fault Tolerant Generator.

**Author Contributions:** Conceptualization, L.S.; methodology, L.S.; software, L.S.; validation, L.S.; formal analysis, L.S.; investigation, L.S.; resources, L.S. and J.A.; data curation, L.S.; writing—original draft preparation, L.S.; writing—review and editing, L.S., J.A. and W.Z.; visualization, L.S.; supervision, L.S.; project administration, L.S.; funding acquisition, L.S.

**Funding:** This research was funded by the National Natural Science Foundation of China (51707110, 51775320, 51875327), Taishan scholars program, and City-University Joint Research project (2018ZBXC197).

**Acknowledgments:** The authors would like to thank Prof. Zhou Bo of Nanjing University of Aeronautics and Astronautics and Byung-il Kwon of Hanyang University for their continuous support and guidance to the authors, especially in this paper.

**Conflicts of Interest:** The authors declare no conflict of interest.

## References

1. Pescini, E.; De Giorgi, M.G.; Francioso, L.; Sciolti, A.; Ficarella, A. Effect of a micro dielectric barrier discharge plasma actuator on quiescent flow. *IET Sci. Meas. Technol.* **2014**, *8*, 135–142. [[CrossRef](#)]
2. Pescini, E.; Francioso, L.; De Giorgi, M.G.; Ficarella, A. Investigation of a Micro Dielectric Barrier Discharge Plasma Actuator for Regional Aircraft Active Flow Control. *IEEE Trans. Plasma Sci.* **2015**, *43*, 3668–3680. [[CrossRef](#)]

3. Campplilongo, S.; De Giorgi, M.G.; Ficarella, A.; Pescini, E.; Sciolti, A.; Dilecce, G. Plasma Actuation to Enhance the Flame Stabilization in a Non-Premixed Lean Microburner. In Proceedings of the 1st Workshop on Nanotechnology in Instrumentation and Measurement (NANOFIM), Lecce, Italy, 24–25 July 2015.
4. Li, W.; Cheng, M. Reliability Analysis and Evaluation for Flux-Switching Permanent Magnet Machine. *IEEE Trans. Ind. Electron.* **2019**, *66*, 1760–1769. [[CrossRef](#)]
5. Zhang, Z.; Yu, L.; Wang, Y.; Wang, Y.; Yan, Y. Overview and design methodology of doubly salient brushless dc generators with stator-field winding. *IET Electr. Power Appl.* **2017**, *11*, 197–211. [[CrossRef](#)]
6. De Giorgi, M.G.; Ficarella, A.; Lay-Ekuakille, A. Cavitation Regime Detection by LS-SVM and ANN with Wavelet Decomposition Based on Pressure Sensor Signals. *IEEE Sensors J.* **2015**, *15*, 5701–5708. [[CrossRef](#)]
7. Francioso, L.; De Pascali, C.; Siciliano, P.; De Giorgi, M.G.; Pescini, E.; Ficarella, A. Aircraft Distributed Flow Turbulence Sensor Network with Embedded Flow Control Actuators. In Proceedings of the 12th IEEE International Conference on Embedded and Ubiquitous Computing, Milano, Italy, 26–28 Aug 2014.
8. Yepes, A.G.; Doval-Gandoy, J.; Baneira, F.; Toliyat, H.A. Speed Estimation Based on Rotor Slot Harmonics in Multiphase Induction Machines Under Open-Phase Fault. *IEEE Trans. Power Electron.* **2018**, *33*, 7980–7993. [[CrossRef](#)]
9. Yepes, A.G.; Doval-Gandoy, J.; Baneira, F.; Toliyat, H.A. Control Strategy for Dual Three-Phase Machines with Two Open Phases Providing Minimum Loss in the Full Torque Operation Range. *IEEE Trans. Power Electron.* **2018**, *33*, 10044–10050. [[CrossRef](#)]
10. Naderi, S.B.; Davari, P.; Zhou, D.; Negnevitsky, M.; Blaabjerg, F. A Review on Fault Current Limiting Devices to Enhance the Fault Ride-Through Capability of the Doubly-Fed Induction Generator Based Wind Turbine. *Appl. Sci.* **2018**, *8*, 2059. [[CrossRef](#)]
11. Mengoni, M.; Zarri, L.; Tani, A.; Parsa, L.; Serra, G.; Casadei, D. High-Torque-Density Control of Multiphase Induction Motor Drives Operating Over a Wide Speed Range. *IEEE Trans. Ind. Electron.* **2015**, *62*, 814–825. [[CrossRef](#)]
12. Yepes, A.G.; Doval-Gandoy, J.; Baneira, F.; Pérez-Estévez, D.; López, O. Current Harmonic Compensation for n-Phase Machines With Asymmetrical Winding Arrangement and Different Neutral Configurations. *IEEE Trans. Ind. Appl.* **2017**, *53*, 5426–5439. [[CrossRef](#)]
13. Rizzoli, G.; Mengoni, M.; Zarri, L.; Tani, A.; Serra, G.; Casadei, D. Comparative Performance Evaluation of Full Bridge, H5 and H6 Topologies for Transformer-Less Solar Converters. *IET Power Electron.* **2019**, *12*, 22–29. [[CrossRef](#)]
14. Mengoni, M.; Amerise, A.; Zarri, L.; Tani, A.; Serra, G.; Casadei, D. Control Scheme for Open-Ended Induction Motor Drives with a Floating Capacitor Bridge Over a Wide Speed Range. *IEEE Trans. Ind. Appl.* **2017**, *53*, 4504–4514. [[CrossRef](#)]
15. El-Refaie, A.M. Motors/generators for traction/propulsion applications: A review. *IEEE Veh. Technol. Mag.* **2013**, *8*, 90–99. [[CrossRef](#)]
16. Zhang, X.; Du, Q.; Ma, S.; Geng, H.; Hu, W.; Li, Z.; Liu, G. Permeance Analysis and Calculation of the Double-Radial Rare-Earth Permanent Magnet Voltage-Stabilizing Generation Device. *IEEE Access* **2018**, *6*, 23939–23947. [[CrossRef](#)]
17. Wei, J.; Deng, Q.; Zhou, B.; Shi, M.; Liu, Y. The control strategy of open-winding permanent magnet starter-generator with inverter-rectifier topology. *IEEE Trans. Ind. Inform.* **2013**, *9*, 983–991. [[CrossRef](#)]
18. Potgieter, J.H.J.; Marguez-Fernandez, F.M.; Fraser, A.G.; McCulloch, M.D. Design optimisation methodology of a high-speed switched reluctance motor for automotive traction applications. In Proceedings of the 8th IET International Conference on Power Electronics, Machines and Drives (PEMD 2016), Glasgow, UK, 19–21 April 2016.
19. Guy, F.; Anthony, G. Integrated starter generator. *IEEE Ind. Appl. Mag.* **2009**, *15*, 26–34.
20. Sim, J.H.; Ahn, D.G.; Kim, D.Y.; Hong, J.P. Three-Dimensional Equivalent Magnetic Circuit Network Method for Precise and Fast Analysis of PM-Assisted Claw-Pole Synchronous Motor. *IEEE Trans. Ind. Appl.* **2018**, *54*, 160–171. [[CrossRef](#)]
21. Dai, W.; Yu, Y.; Hua, M.; Cai, C. Voltage regulation system of doubly salient electromagnetic generator based on indirect adaptive fuzzy control. *IEEE Access* **2017**, *5*, 14187–14194. [[CrossRef](#)]
22. Chen, Z.; Wang, H.; Yan, Y. A doubly salient starter-generator with two-section twisted-rotor structure for potential future aerospace application. *IEEE Trans. Ind. Electron.* **2012**, *59*, 3588–3595. [[CrossRef](#)]

23. Zhao, Y.; Wang, H.; Li, D.; Qian, R. Comparative Research of Wound Field Doubly Salient Generator with Different Rectifiers. *IEEE Trans. Ind. Inform.* **2018**, *14*, 4851–4863. [[CrossRef](#)]
24. Xiao, D.; Shi, L.; Guo, Y.; Han, Z.; Zhou, X. Investigation of the working mechanism and characteristics of dual-mode doubly salient starter generator with variable winding. *IET Electr. Power Appl.* **2018**, *12*, 1240–1246. [[CrossRef](#)]
25. Lee, C.H.T.; Chau, K.T.; Liu, C.; Chan, C.C. Overview of magnetless brushless machines. *IET Electr. Power Appl.* **2018**, *12*, 1117–1125. [[CrossRef](#)]
26. Yu, L.; Zhang, Z.; Chen, Z.; Yan, Y. Analysis and verification of the doubly salient brushless DC generator for automobile auxiliary power unit application. *IEEE Trans. Ind. Electron.* **2014**, *61*, 6655–6663. [[CrossRef](#)]
27. Taras, P.; Li, G.J.; Zhu, Z.Q. Comparative study of fault-tolerant switched-flux permanent-magnet machines. *IEEE Trans. Ind. Electron.* **2017**, *64*, 1939–1948. [[CrossRef](#)]
28. Bu, F.; Liu, H.; Huang, W.; Xu, H.; Shi, K. Optimal-Third-Harmonic-Injection-Based Control for Five-Phase Dual-Stator Winding Induction Generator DC Generating System. *IEEE Trans. Ind. Electron.* **2018**, *65*, 9124–9134. [[CrossRef](#)]
29. Chinmaya, K.A.; Singh, G.K. Performance evaluation of multiphase induction generator in stand-alone and grid-connected wind energy conversion system. *IET Renew. Power Gen.* **2018**, *12*, 823–831. [[CrossRef](#)]
30. Zhao, Y.; Wang, H.; Xiao, L. Investigation of fault-tolerant capability of five-phase doubly salient electromagnetic generator. *IET Electr. Power Appl.* **2014**, *9*, 80–93. [[CrossRef](#)]
31. Jun-Hyung, K.; Yuan-Wu, J.; Sang-Moon, H. Analysis of a Vibrating Motor Considering Electrical, Magnetic, and Mechanical Coupling Effect. *Appl. Sci.* **2019**, *9*, 1434.
32. Shi, L.; Zhou, B. Analysis of a new five-phase fault-tolerant doubly salient brushless DC generator. *IET Electr. Power Appl.* **2016**, *10*, 633–640.
33. Cheng, M.; Han, P.; Hua, W. General airgap field modulation theory for electrical machines. *IEEE Trans. Ind. Electron.* **2017**, *64*, 6063–6074. [[CrossRef](#)]
34. Francioso, L.; De Pascali, C.; Casino, F.; Siciliano, P.; De Giorgi, M.G.; Campilongo, S.; Ficarella, A. Embedded sensor/actuator system for aircraft active flow separation control. In Proceedings of the XVIII AISEM Annual Conference, Trento, Italy, 3–5 February 2015.
35. Tang, R. *Theory and Design of Modern Permanent Magnet Machines*; Mechanical Industry Press: Beijing, China, 2016; p. 298.
36. Shi, L.; Zhou, B. Armature Reaction Analysis of a New Four-phase Fault-tolerant Doubly Salient Wound-Field Generator. *IEEE Trans. Appl. Super.* **2016**, *26*, 0612005. [[CrossRef](#)]



© 2019 by the authors. Licensee MDPI, Basel, Switzerland. This article is an open access article distributed under the terms and conditions of the Creative Commons Attribution (CC BY) license (<http://creativecommons.org/licenses/by/4.0/>).